View metadata, citation and similar papers at core.ac.uk

brought to you by CORE

provided by Queen Mary Research Online

This document is confidential and is proprietary to the American Chemical Society and its authors. Do not copy or disclose without written permission. If you have received this item in error, notify the sender and delete all copies.

Organic Single-Crystalline p-n Heterojunctions for High-Performance Ambipolar Field-Effect Transistors and Broadband Photodetectors

Journal:	*ACS Applied Materials & Interfaces*
Manuscript ID	am-2018-128328.R2
Manuscript Type:	Article
Date Submitted by the Author:	01-Nov-2018
Complete List of Authors:	Zhao, Xiaoming; Queen Mary University of London, Liu, Tianjun; Queen Mary University of London Liu, Hongli; Tianjin University Wang, Shirong; School of Chemical Engineering and Technology, Tianjin University, Li, Xianggao; Tianjin University, Zhang, Yuteng; Tianjin University Hou, Xueyan; Queen Mary University of London Liu, Zilu; Queen Mary University of London Shi, Wenda; Queen Mary Univeristy of London, Physics Dennis, Terence; Queen Mary University of London, School of Physics and Astronomy

SCHOLARONE™
Manuscripts

Organic Single-Crystalline p-n Heterojunctions for High-Performance Ambipolar Field-Effect Transistors and Broadband Photodetectors

Xiaoming Zhao,[1‡] Tianjun Liu,[1‡] Hongli Liu,[2,3] Shirong Wang,[2,3] Xianggao Li,[2,3] Yuteng Zhang,[2,3] Xueyan Hou,[1] Zilu Liu,[1] Wenda Shi[1] and T. John S. Dennis[1]**

[1] Materials Research Institute and School of Physics and Astronomy, Queen Mary University of London, Mile End Road, London E1 4NS, United Kingdom
[2] School of Chemical Engineering and Technology, Tianjin University, 300072 Tianjin, China.
[3] Collaborative Innovation Center of Chemical Science and Engineering (Tianjin), 300072 Tianjin, China.

* Corresponding authors: Shirong Wang (email: wangshirong@tju.edu.cn) and T. John S. Dennis (email: j.dennis@qmul.ac.uk)

‡ These authors contributed equally.

KEYWORDS: Single-crystalline heterojunction; ambipolar charge transport; broadband; organic photodetector; organic field-effect transistors.

ABSTRACT: Organic semiconducting single crystals are ideal building blocks for organic field-effect transistors (OFETs) and organic photodetectors (OPDs) because they can potentially exhibit the best charge transport and photoelectric properties in organic materials. Nevertheless, it is usual for single-crystal OFETs to be built from one kind of organic material in which the dominant transport is either electron or hole; such OFETs showing unipolar charge transport. Furthermore, single-crystal OPDs present high performance only in restricted regions because of the limited absorption of one-component single crystals. In an ideal situation, devices which comprise both

electron and hole transporting single crystals with complementary absorptions, like single-crystalline p-n heterojunctions (SCHJs), can permit broadband photo-response and ambipolar charge transport. In this paper, a solution-processing crystallization strategy to prepare an SCHJ composed of C_{60} and 6,13-bis(triisopropylsilylethynyl)pentacene (TIPS-PEN) was shown. These SCHJs demonstrated ambipolar charge transport characteristics in OFETs with a balanced performance of 2.9 cm^2 V^{-1} s^{-1} for electron mobility and 2.7 cm^2 V^{-1} s^{-1} for hole mobility. This demonstration is the first of single-crystal OFETs in which both electron and hole mobilities were over 2.5 cm^2 V^{-1} s^{-1}. OPDs fabricated upon as-prepared SCHJs exhibited highly-sensitive photo-conductive properties ranging from ultraviolet to visible and further to near-infrared regions as a result of complementary absorption between C_{60} and TIPS-PEN; thereby attaining the photo-responsivities amongst the highest-reported values within the organic photodetectors. This work would provide valuable references for developing novel SCHJ systems to achieve significant progress in high-performance ambipolar OFETs and broadband OPDs.

Introduction

Recently, continuous research attention has been drawn to organic field-effect transistors (OFETs) for lightweight and deformable electronic applications like photodetectors,[1] sensors,[2] displays,[3] and circuits.[4] Included in these, organic photodetectors (OPDs), which translate optical signals into electrical signals, occupy an essential position in optical interconnection techniques, light-wave communications,

and high-resolution imaging.[5–10] Since single crystals are free of molecular disorder and grain boundary, they are considered to be a favorable charge transport medium for OPD and OFET devices.[11–14] High-performance single-crystal electronics are generally constructed from one kind of organic semiconducting crystals in which either electron or hole transport is dominant. Devices which comprise both p-type and n-type single crystals like single-crystalline p-n heterojunctions can instinctively allow more functions such as broadband photo-response and ambipolar charge transport.[15]

Two-dimensional materials such as graphene have been appearing as promising contenders within p-n heterojunction for photoelectronic and electronic applications.[16,17] Organic semiconductors are dissimilar to 2D nanosheets which comprise an atomic layer, in that they can form quasi-2D single crystals in which molecules are bonded weakly by van der Waals interaction rather than by covalent bonds.[18] Therefore, they have the potential for solution processing at room temperature as well as for chemical modification.[18] Nevertheless, literature has shown only a small number of pioneering studies on SCHJs as a result of difficulty in obtaining such a highly-ordered nanostructure of this kind. Physical vapor transport (PVT) method and one-pot mixed-solution crystallization method have been demonstrated to successfully prepare organic SCHJ p-n systems.[15,19] However, there are drawbacks with the PVT technique in that it needs complex equipment and is energy consuming, whereas the one-pot mixed-solution crystallization technique needs one crystal to grow quickly and the other to grow particularly slowly, so as to avert mutual disturbance of these two crystals in order to obtain overlapping bilayer single crystals instead of a combination

of two solids.[15] It was reported that this one-pot crystallization technique successfully prepared only two specific p-n pairs (DPP-PR/C_{60} and C8BTBT/C_{60}) up to the present time as a result of this stringent requirement. Due to such limits, the device performance in such system remains moderate. As summarized in **Table 1**, for reported single crystal-based ambipolar OFETs, the hole and electron mobility are usually low and unbalanced; Single-crystal based OFETs with both hole and electron mobility exceeding 1 cm^{-2} V^{-1} s^{-1} is rarely seen in the literature.[12,15,20–26] Single-crystal OPDs have been demonstrated to exhibit higher photo-responsivity than polycrystalline thin film devices, as shown in **Table 2**. However, due to the limited absorption of one-component single crystals, these single-crystal OPDs present high performance only in limited regions. Therefore, to achieve significant advancements in both high-performance ambipolar OFETs and broadband OPDs, developing facile crystallization method to prepare novel SCHJ p-n nanostructures is urgently necessary.

In this paper, a facile two-step aligned crystallization strategy is reported; this is for the purpose of acquiring single-crystalline p-n heterojunctions which comprise two "benchmark" organic semiconductors, being C_{60} (n-type) and 6,13-bis(triisopropylsilylethynyl)pentacene (TIPS-PEN, p-type) and also to study its application in ambipolar OFETs and broadband photodetectors. The SCHJs presented herein show a balanced ambipolar charge transport with an average performance of (2.44 ± 0.222) cm^2 V^{-1} s^{-1} for electron mobility (μ_e) and (2.17 ± 0.309) cm^2 V^{-1} s^{-1} for hole mobility (μ_h) which demonstrate the first of single crystal OFETs with both electron and hole mobilities greater than 2 cm^2 V^{-1} s^{-1}. Photodetectors based upon as-

prepared SCHJs offer a highly-sensitive photo-response with fast photo-switching and repeatable characteristics in broadband UV-Vis-NIR regions due to the complementary absorption between C_{60} and TIPS-PEN; furthermore, the photo-responsivities achieved here are among the highest values in the reported organic photodetectors. The presented work here is a valuable reference for the development of novel single-crystalline heterojunction nanostructures and the exploration of the fundamental studies on organic electronics at new organic/organic interfaces and enables significant advancements in high-performance ambipolar OFETs and broadband OPDs.

Result and Discussion

TIPS-PEN and C_{60} are among the most extensively-utilized p-type and n-type semiconductors respectively with both μ_h (TIPS-PEN) and μ_e (C_{60}) greater than 5 $cm^2 V^{-1} s^{-1}$ in single-crystal OFETs.[27,28] Furthermore, they demonstrate superior performance in several photoelectronic devices like hybrid perovskite solar cells,[29] OPVs, [30–32] and OLEDs.[33] Therefore, C_{60} and TIPS-PEN, on this work, were utilized to grow single-crystalline p-n heterojunctions. **Figure S1** (Supporting Information) depicts the molecular structures of C_{60} and TIPS-PEN, whereas **Figure 1a** illustrates the fabrication of SCHJs *via* a two-step aligned crystallization technique. Two-step crystallization method using orthogonal solvents have been reported to successfully prepare high-quality SCHJs for optoelectronics and FET-based memory devices and the devices based on the SCHJs prepared by this two-step crystallization method exhibit superior performance due to the high-quality interface formed by this method.[20,34] In addition, this method is also called interfacial solution-processed crystallization

method, where a second layer of single crystals forms on the interface with the first single crystal layer, leading to bilayered single-crystalline structures.[20] Therefore, this two-step crystallization method can offer high-quality interface. For aligned crystal growth, a preferential drying direction is imposed upon the drop casted solution in order to control the direction of the crystal growth which is attained by placing the substrate in a Petri dish at an angle of 5° to the horizontal line on a hot plate at a temperature of (25±1) °C. Following this procedure, the lid was replaced immediately in order to trap the solvent vapor, thereby creating a vapor-saturated condition within the Petri dish. Firstly, this technique was applied to grow C_{60} ribbons by drop-casting a C_{60} solution in an *o*-dichlorobenzene (ODCB) solvent; subsequently we rotated the substrates by 90°, and following this, we drop-casted TIPS-PEN solution using the same technique as aforementioned. In this way, TIPS-PEN single crystals formed over the top of the first due to slow solvent evaporation; this results in bilayer structures as depicted in **Figure S2** (Supporting Information)**.** Avoidance of damaging the first layer in the crystallization process of second layer is a principal challenge in the second stage, the key to this being obviously the choice of solvent for the second layer.[35] Thus, 4-methyl-2-pentanone, which can effectively dissolve TIPS-PEN but cannot dissolve C_{60} , is chosen as the solvent to grow TIPS-PEN single crystals without dissolving the first layer. In order to remove the remaining solvents, the substrate was treated by vacuum annealing following the TIPS-PEN crystal growth. Consequently, as shown in **Figure S3** (Supporting Information), a bilayer structure having both ribbons of a few microns wide was acquired.

As shown in **Figure 1c and d,** the crystals were studied by energy dispersive spectrum (EDS) on a scanning electron microscope (SEM) to identify the chemical composition of the overlapping bilayer in **Figure 1b.** It was distinctly demonstrated by element mapping of Si (TIPS-PEN) and C (both TIPS-PEN and C_{60}) that the TIPS-PEN ribbon was over the top of the C_{60} ribbon to form a single-crystalline heterojunction. Atomic force microscopy (AFM) height profile was employed in order to study the thickness of the overlapping SCHJ as illustrated in **Figure 1e** and it was shown that the thickness of one SCHJ was 160 nm including 71 nm of C_{60} layer and 89 nm of TIPS-PEN layer. As illustrated in **Figure 1f and g**, crystallography studies of the bilayers was performed *via* select area electron diffraction (SAED) on transmission electron microscopy (TEM). Two groups of diffraction spots (blue and yellow circles) in **Figure 1g** were shown by the SAED of the bilayers, indicating two different single crystals. This is similar to the SAED patterns reported for C_{60}/DPP-RP and CuPc/F_{16}CuPc single-crystalline heterojunctions, where two sets of diffraction spots were also observed.[15,19] It should be noted that the growth of TIPS-PEN crystal on top of C_{60} crystal is not the epitaxial growth; the lattice mismatch of both crystals is unable to provide significant condition for epitaxial growth.[19] We indexed the SAED pattern of TIPS-PEN with a triclinic crystal system, and the cell dimensions of TIPS-PEN ribbon crystal are a = 7.58 Å, b = 7.72 Å and c = 16.81 Å, which is in accordance well with the reported literature.[36] A face center cubic (FCC) crystal structure having a lattice constant of a = 1.414 nm was indexed by the SAED pattern for the C_{60} ribbon crystals, according with this value of pristine C_{60} crystals (1.415 nm).[37] It is shown by the

evidence of the AFM, EDS OM, SAED, SEM and TEM that the SCHJ of C_{60} and TIPS-PEN ribbon crystals were indeed obtained.

Our p-n heterojunctions' single-crystalline nature demonstrates their high quality and possible utilization in high-performance ambipolar OFETs; therefore, we artificially designed an asymmetric device structure having a top-contact and bottom-gate configuration in order to study their ambipolar charge transport properties. The schematic diagram and the corresponding SEM image of the as-fabricated OFETs are respectively depicted in **Figure 2a and b.** Three different circuit models will be induced while applying different source and drain pairs because of the asymmetric device structure. When S1/D1 or S2/D2 is utilized as a source and drain pair, the performance of the device will be dominated by the charge transport through single-component ribbon crystals (C_{60} or TIPS-PEN ribbon), but when S1/D2 or S2/D1 is used as the source and drain electrodes, the charge transport performance is determined by single-crystalline heterojunction. Firstly, to study the charge transport through single-crystalline heterojunction, we selected S1/D2 as the electrode pair. **Figure 2c and d** depicts the typical transfer characteristics of devices, showing V-shaped curves in which both arms correspond to hole transport and electron transport, indicating the ambipolar charge transport characteristics in SCHJs. The excellent gate modulation was confirmed by the output characteristics (**Figure S4 and S5**, Supporting Information). **Figure S6 and S7** illustrates the histograms of electron and hole mobility acquired from 50 devices based on as-prepared SCHJs. Based on these, an average μ_h of (2.17 ± 0.309) $cm^2\ V^{-1}\ s^{-1}$ and an average μ_e of (2.44 ± 0.222) $cm^2\ V^{-1}\ s^{-1}$ were obtained on as-

fabricated SCHJ OFETs. Secondly, we selected S1/D1 as the electrode pair to examine the charge transport properties of individual TIPS-PEN ribbon crystal. In this condition, only p-channel devices exhibited effective field-effect mobility. 50 devices were studied and an average μ_h of (2.83 ± 0.402) $cm^2\ V^{-1}\ s^{-1}$ were achieved as shown in **Figure S8**. Thirdly, we selected S2/D2 as the electrode pair to study the charge transport characteristics of individual C_{60} ribbon crystal. On the contrary, effective field-effect mobility can only be extracted from n-channel devices and we achieved an average μ_e of (2.74 ± 0.266) $cm^2\ V^{-1}\ s^{-1}$ (**Figure S9**). We found that compared to the hole and electron mobility of the individual ribbon crystal, the mobility values of the single-crystalline p-n heterojunctions are comparable but slightly lower. This phenome was also observed by Bao *et al*.[24] In addition to the different channel coverage, this disparity may be due to the slight incorporation of one molecule inside the crystal of the other and therefore potential crystal lattice disruption.[24]

When S1/D2 was selected as the electrode pair, the conductive channel contains C_{60}, the SCHJ, and TIPS-PEN. The schematic band diagram of the charge transport process is shown in **Figure S10**. When bias voltage is applied, band bending happens at the interface between C_{60} and TIP-PEN. As shown in **Figure S10b**, when (V_{GS} - V_T) = 0, the energy difference between the LUMO of C_{60} and HOMO of TIPS-PEN is defined as V_{b1}, and the energy difference between the HOMO of TIPS-PEN and the HOMO of C_{60} is defined as V_{b2}. As shown in **Figure S10c**, when (V_{GS} - V_T) > 0 (n-channel operation mode), V_{b1} decreases by continuously increasing V_{GS}, and the probability that the electrons at the TIPS-PEN HOMO hopping to C_{60} LUMO increases,

leading to increases of electron concentration in C_{60} and hole concentration in TIPS-PEN accordingly. In this case, IDS of this n-channel operation mode will increase. While for the p-channel operation mode where (V_{GS} - V_T) < 0 (**Figure S10d**), V_{b2} decreases when the value of V_{GS} is increasing. In this case, there is a large amount of hole accumulation at the valence band of TIPS-PEN. Due to the decreasing V_{b2}, the holes at the valence band of TIPS-PEN recombine, at the interface, with the electrons in C_{60} HOMO, forming the recombination current. This recombination current increases when V_{GS} is more negative, leading to the field effect.

For ambipolar FETs, balanced electron and hole mobility are desirable, because this is important for a broad range of electronic devices such as complementary circuits and light-emitting field-effect transistors.[38] The maximum performance we achieved in SCHJ based OFETs is a balanced hole and electron mobility of 2.71 $cm^2\ V^{-1}\ s^{-1}$ and 2.89 $cm^2\ V^{-1}\ s^{-1}$, respectively. To better demonstrate the improvement of present SCHJs for ambipolar OFETs, we make a comparison of some recently reported SCHJs applied in OFETs. The donor-acceptor system and the corresponding parameters of the OFETs based on these SCHJs are tabulated in **Table 1**. It clearly shows that most of the SCHJs present relatively low ambipolar charge transport mobilities with both hole and electron mobility below 1 $cm^2\ V^{-1}\ s^{-1}$. But there are two exceptions: $CdCl_3/C_{60}$ SCHJ presents an electron mobility as high as 1.28±0.41 $cm^2\ V^{-1}\ s^{-1}$ in OFETs but its hole mobility is not given;[20] While DPTTA/F_2TCNQ gives OFETs a relatively higher hole mobility of 1.57 $cm^2\ V^{-1}\ s^{-1}$ but its electron mobility is about 4 times lower (0.47 $cm^2\ V^{-1}\ s^{-1}$).[21] The TIPS-PEN/C_{60} SCHJ in the present work, which gives ambipolar

OFETs balanced charge transport properties with average hole mobility of 2.17 $cm^2 V^{-1} s^{-1}$ and average electron mobility of 2.44 $cm^2 V^{-1} s^{-1}$, is the first demonstration for SCHJ-based OFETs with both hole and electron mobility above 2 $cm^2 V^{-1} s^{-1}$, making it a potential candidate for high-performance ambipolar OFETs.

TIPS-PEN/C_{60} SCHJ is endowed with high-mobility ambipolar charge transport property, providing considerable potential in high-performance photoelectronic devices like organic photodetectors. The absorption spectra of TIPS-PEN/C_{60} single-crystalline heterojunctions, pristine TIPS-PEN single crystal, and C_{60} single crystal are depicted in **Figure 3d**, whereas the TIPS-PEN single crystals' spectrum present a dominant band centered at 653 nm with absorption being extended to the NIR region, and also two fractionally weaker shoulder bands having peaks at 547 and 598 nm outside the C_{60} single crystals' spectral coverage. The TIPS-PEN/C_{60} SCHJ exhibits broadband absorption in the region of 350-750 nm as a result of this complementary absorption enabling it to be a possible candidate for broadband photodetection.

As depicted in **Figure 3a and b**, a discrete heterojunction was employed to construct a photodetection device which used the asymmetrical (ITO/Al) electrodes in order to reduce the energy barrier between the semiconducting crystals and the electrodes, thereby effectively easing the charge injection.[39] The reason for this, as depicted in **Figure 3c**, is that the Al's work function being a good match with the LUMO energy of the n-type C_{60} while the ITO work function being a good match with the HOMO energy level of the p-type material TIPS-PEN.

The diode characteristic and rectifying properties are typical characteristics of p-n heterojunctions.[40] In a typical p−n heterojunction, rectification results from the potential barrier formed at the interface between two types of semiconductor materials, p- and n-types.[40] In the forward bias, the current increased with increase in the applied bias due to decrease in the potential barrier while in the reverse bias only a small amount of current can flow as the barrier height is increased with the applied bias.[40] **Figure 3e** illustrates the comparison of the current-voltage (*I-V*) curves of as-fabricated photodetectors under dark and upon illumination by 1.5 mW cm^{-2} laser with different wavelengths at room temperature. The TIPS-PEN/C_{60} SCHJ device, as expected, presents typical diode characteristics and demonstrates good rectifying property, indicating that high-quality heterojunctions are formed between TIPS-PEN and C_{60} ribbons.

Meanwhile, photodetectors based on a pure TIPS-PEN or pure C_{60} single crystal were also studied under the identical condition for comparison. **Figure 3e** shows how a weak dark current (5.7 nA at 30 V bias) was given by this SCHJ photodetector, but when illuminated by the laser of different wavelengths, there was a considerable increase in the photo currents. In order to evaluate the photodetectors' performances quantitatively, their spectral responsivity (*R*) was calculated according to Equation (1):

$$R = \frac{I_{light} - I_{dark}}{PS} \qquad (1)$$

where I_{light} is the current when illuminated by the laser, I_{dark} is the current under dark condition, *P* is the incident power density, and *S* is the effective illuminated area.

With regard to the SCHJ photodetector, *R* was calculated as 165.5 A W^{-1} at 350 nm, 149.6 A W^{-1} at 650 nm and 22.5 A W^{-1} at 720 nm when applying a bias voltage of 30 V (**Figure 3f**), thereby showing the broadband photo-response attributes of SCHJ OPDs. Contrastingly, the *R* for the pure C_{60} single crystal photodetector was calculated as being significantly less at 96.7 A W^{-1} at 350 nm, 16.6 A W^{-1} at 650 nm and 8.9 A W^{-1} at 720 nm. Likewise, photodetectors based upon the TIPS-PEN single crystal indicate weaker photo-response attributes than do SCHJ devices, having an *R* of 79.9 A W^{-1} and 114.5 A W^{-1} respectively, attained at 350 nm and 650 nm; furthermore, negligible photo-response was detected in the NIR area**.** It was revealed by all of these results that the single-crystalline heterojunction formed between C_{60} and TIPS-PEN single crystals led to a considerable enhancement in the response in the ultraviolet region and also provided the extension of response to the visible and near-infrared regions.

Literatures reveals that with regard to the heterojunction photodetectors, when applying a bias voltage, the heterojunction interface is able to improve the excitons' dissociation (photogenerated in both TIPS-PEN and C_{60} single crystals) into more separated free charge carriers, thereby resulting in the photocurrent improvement of the SCHJ photodetector.[41–43] The deeper-lying LUMO level of C_{60} is able to transfer the photogenerated electrons from TIPS-PEN to C_{60}, thereby, leading to spatial separations of holes and electrons. Resultantly, the carrier recombination was suppressed and the holes' lifetime was extended in TIPS-PEN single crystals, leading to greater enhancement in the photodetector performance.

Figure 4a depicts the SCHJ device's spectral responsivity as function of the bias voltage, which is also shown in a contour (**Figure 4b**). It is distinctly observable that the device responsivity is considerably improved by increasing bias voltage, resulting in the sensitive identification of NIR and fully-visible light at bias voltages greater than 10V. Furthermore, **Figure 3f** shows that the spectral responsivity displays clear absorption peaks coincident with the peaks observed in the SCHJs**'** absorption spectrum**. Figure 4c** depicts time-resolved current response in different illumination conditions with and without illumination at an applied bias of 30V. The "on" and "off" states maintain the same current level for several cycles under illumination of identical wavelength, thereby showing these photodetectors' excellent stability and reversibility. Additionally, it is demonstrated by the analysis of an enlarged photo-response process involving one rise and one reset that the SCHJ devices have fast photo-switching attributes with both rising and reset response times under one second (**Figure 4d**).

The performance of representative organic photodetectors is summarized in **Table 2** which indicates that high responsivities are normally obtained in single crystal devices; for example, C8-BTBT single crystal device (124 A W^{-1} under 365 nm UV illumination) and C_{60} single crystal device (90.4 A W^{-1} under 360 nm UV illumination);[44,45] nevertheless, as the result of the limited absorption regions of these single crystals, the photodetectors on which they are based demonstrate only high performance in restricted regions. The current TIPS-PEN/C_{60} photodetectors exhibit higher responsivities than the majority of these devices;[44–58] furthermore, they

demonstrate highly-sensitive photo-response from NIR to Vis to UV regions, showing their excellence for broadband UV-Vis-NIR photodetection

Conclusion

In summary, a simple solution-processed crystallization strategy was developed to prepare a novel organic SCHJ system comprising TIPS-PEN and C_{60}. TIPS-PEN/C_{60} single-crystalline heterojunctions present balanced high-performance ambipolar charge transport property in OFETs and highly-sensitive broadband UV-Vis-NIR responsivity in OPDs. The device performances of presented SCHJ were among the highest for single crystal based ambipolar OFETs and OPDs, respectively. The presented work here is a valuable reference for the development of novel single-crystalline heterojunction nanostructures and the exploration of the fundamental studies on organic electronics at new organic/organic interfaces and enables significant advancements in high-performance ambipolar OFETs and broadband OPDs.

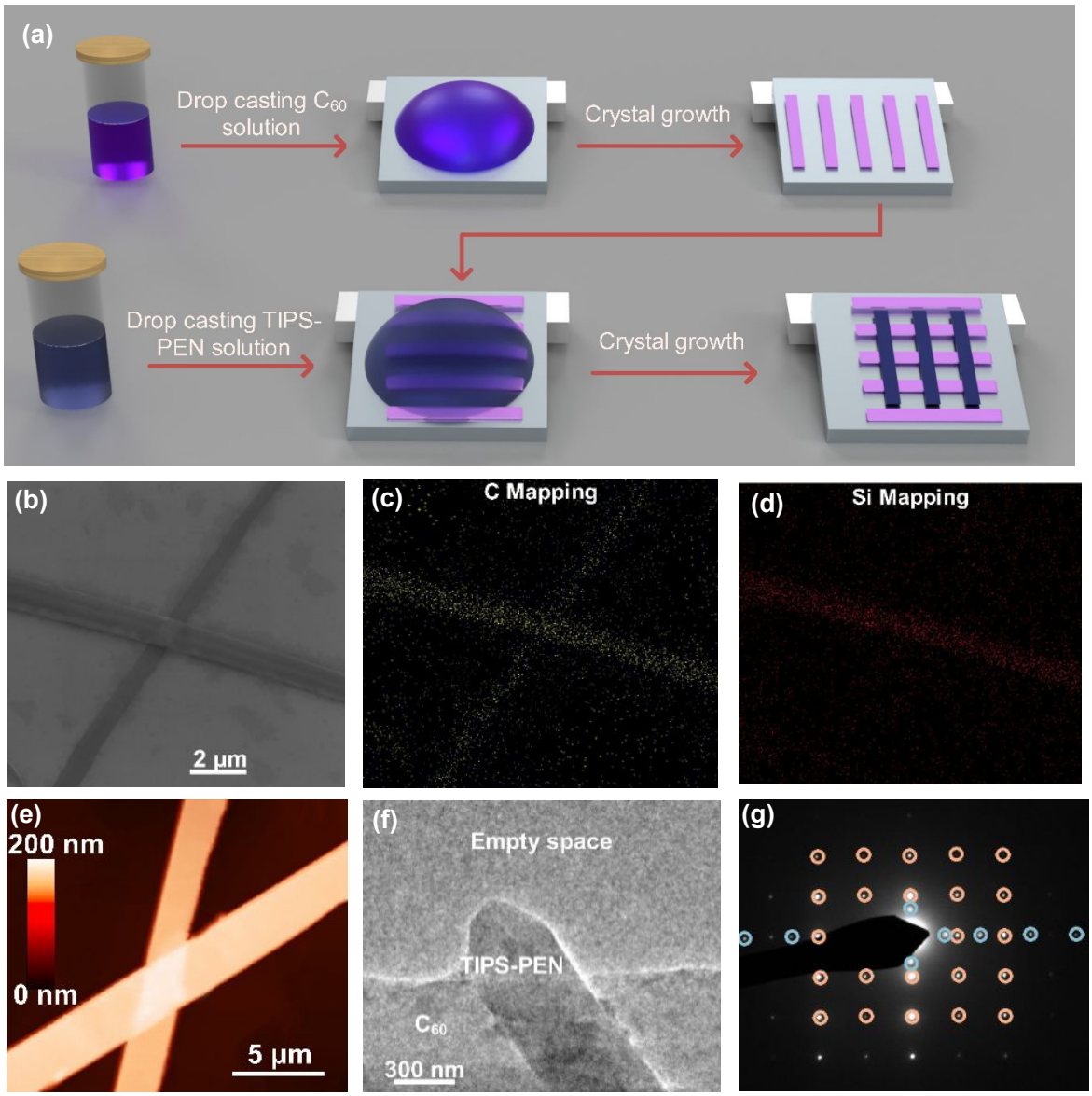

Figure 1 (a) Schematic diagram of preparation of TIPS-PEN/C_{60} single-crystalline heterojunctions; (b) SEM image, associate element mappings of (c) C and (d) Si using EDS and (e) AFM image of one single-crystalline p-n heterojunction; (f) TEM image and (g) associate electron diffraction pattern of one SCHJ.

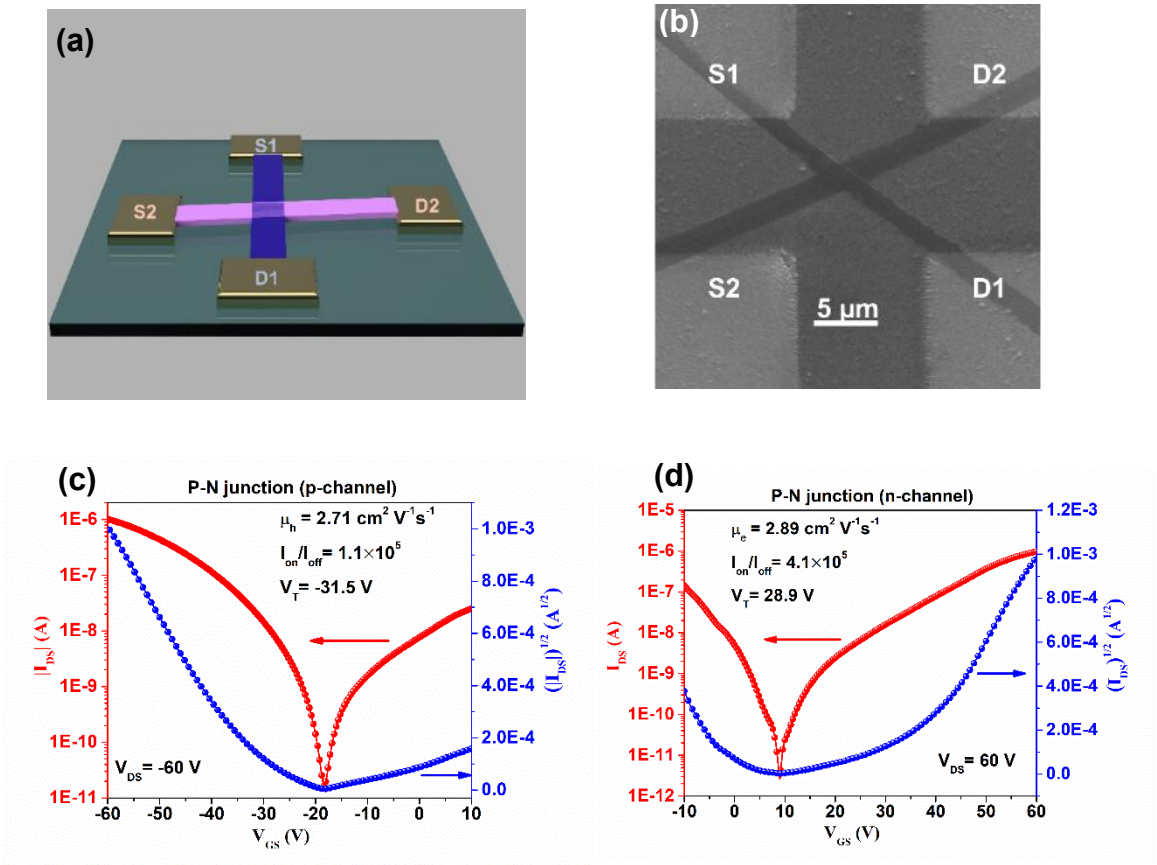

Figure 2 (a) Schematic diagram and (b) SEM image of as-fabricated OFET device based on TIPS-PEN/C_{60} SCHJ. Typical transfer curves of s as-fabricated OFET device in (c) p-channel operation mode and (d) n-channel operation mode, respectively.

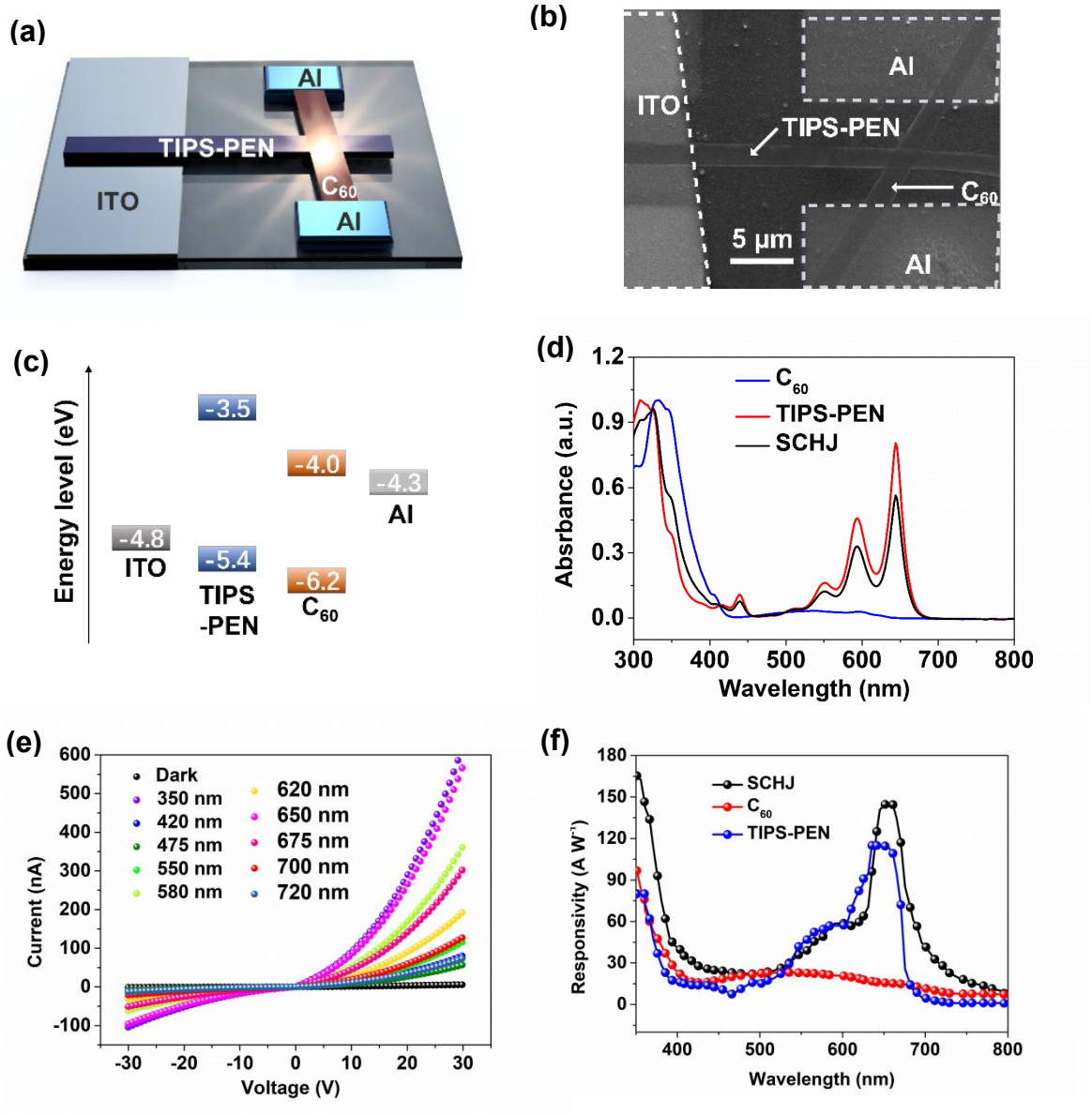

Figure 3 (a) Schematic configuration and (b) SEM image of a single p-n heterojunction device; (c) Energy level alignment of the device structures; (d) Absorption spectra of C_{60} single crystals, TIPS-PEN single crystals and C_{60}/TIPS-PEN single-crystalline heterojunctions; (e) Current-voltage (*I–V*) characteristic of a single TIPS-PEN/C_{60} single-crystalline heterojunction device in dark and under laser illuminations; (f) Spectral responsivity of C_{60}, TIPS-PEN and SCHJ devices.

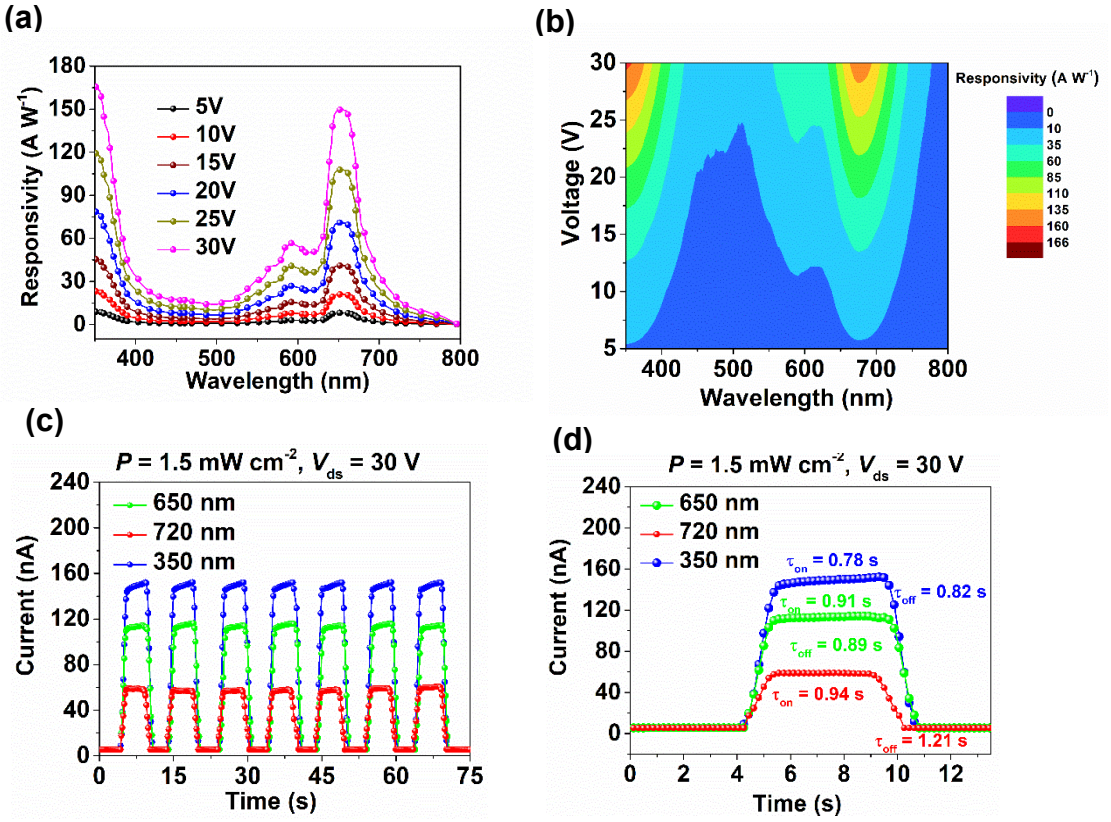

Figure 4 (a) Spectral responsivity of the SCHJ devices measured as a function of applied bias voltage; (b) Responsivity of the SCHJ device shown in 2D contour plot; (c) time-resolved photo-response and (d) an analysis of one response and reset process of SCHJ device under different laser illuminations.

Table 1 Comparison of the device performance for the TIPS-PEN/C_{60} SCHJ and other characteristic organic SCHJs.

Donor	Acceptor	μ_h [cm^{-2} V^{-1} s^{-1}]	μ_e [cm^{-2} V^{-1} s^{-1}]	P_{in} [mW cm^{-2}]	J_{SC} [mA cm^{-2}]	V_{OC} [V]	*FF*	*PCE* [%]	Ref.
$CdCl_3$	C_{60}	NA	1.28 ± 0.41	NA	NA	NA	NA	NA	[20]
DPTTA	TCNQ	0.03	0.04	NA	NA	NA	NA	NA	[59]
DPTTA	F_2TCNQ	1.57	0.47	NA	NA	NA	NA	NA	[21]
DPTTA	DTTCNQ	0.77	0.24	NA	NA	NA	NA	NA	[60]
CuPc	F_{16}CuPc	0.05	0.07	100	0.054	0.35	0.36	0.007	[19]
CuPc	H_2TPyP	NA	NA	5.51	0.029	0.64	0.23	0.08	[23]
C8-BTBT	C_{60}	0.16	0.17	NA	NA	NA	NA	NA	[24]
DPP-PR	C_{60}	0.0061	0.59	100	1.56	0.56	0.38	0.33	[15]
DPTTA	C_{60}	0.3	0.01	10	0.3	0.48	0.18	0.27	[25,26]
DPTTA	C_{70}	0.07	0.06	10	0.002	0.17	0.15	0.0005	
TPB	C_{60}	0.066	0.087	100	1.152	0.53	0.39	0.24	[12]
TIPS-PEN	C_{60}	2.71	2.89	100	4.37	0.52	0.59	1.34	Present work

Table 2 Comparison of the device performance for the TIPS-PEN/C_{60} SCHJ photodetectors and other characteristic OPDs.

Photodetector	Light source [nm]	P_{in} [mW cm^{-2}]	$\|V_{ds}\|$ [V]	R [A W^{-1}]	Ref.
Pentacene	365	1.55	50	50	46
CuPc	365	1.55	50	2	46
Spiro-4p-CPDT	370	NA	20	25	47
Spiro-DPSP	370	0.127	10	1	48
C_{60}	360	4.38	10	90.4	44
6T	365	1.5	50	2.4	49
BPTT	380	1.55	50	82	50
C8-BTBT	365	1.0	30	124	45
	365	0.2	30	117	
F8T2	405	3	10	0.0004	51
Graphene	532	NA	0.02	8.61	52
Pentacene	650	5	50	0.45	46
Pentacene/C_{60} PHJ	580	NA	10	0.122	53
P3HT/$PC_{61}BM$ BHJ	468	40	1	0.1	54
MEH-PPV/$PC_{61}BM$ BHJ	488	0.001	4	0.14	55
F8T2/$PC_{61}BM$ BHJ	460	9	10	0.67	56
PDDTT/$PC_{61}BM$ BHJ	800	0.22	0.5	0.1	57
PTT/$PC_{61}BM$ BHJ	800	NA	5	0.267	58
TIPS-PEN/C_{60} SCHJ	350	1.5	30	165.5	Present work
TIPS-PEN/C_{60} SCHJ	650	1.5	30	149.6	Present work
TIPS-PEN/C_{60} SCHJ	720	1.5	30	22.5	Present work

TOC

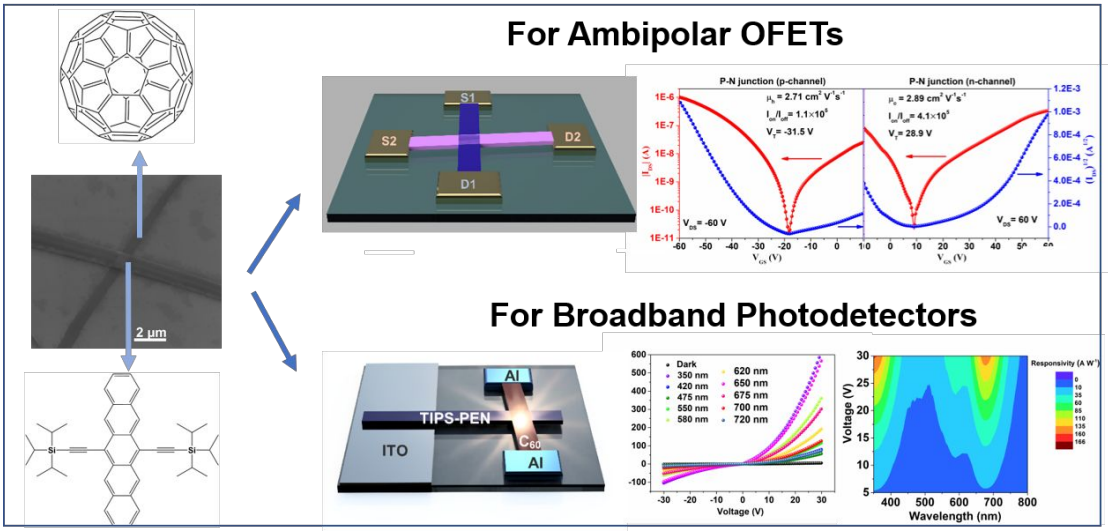
For Ambipolar OFETs
S1
S2
D1
D2
P-N junction (p-channel)
P-N junction (n-channel)
2 μm
For Broadband Photodetectors
Al
TIPS-PEN
ITO
Al
Dark
350 nm
420 nm
475 nm
550 nm
580 nm
620 nm
650 nm
675 nm
700 nm
720 nm
Voltage (V)
Wavelength (nm)
Responsivity (A W⁻¹)

ASSOCIATED CONTENT

Supporting Information.

Experimental Section; Molecular structures of TIPS-PEN and C_{60}; OM image and SEM image of bulk single-crystalline p-n heterojunctions. Output characteristics of SCHJ OFETs in p-channel operation mode; Output characteristics of SCHJ OFETs in n-channel operation mode; Histograms of hole and electron mobilities acquired from 50 SCHJ OFETs.

AUTHOR INFORMATION

Corresponding Author

*Email: Shirong Wang (email: wangshirong@tju.edu.cn), T. John S. Dennis (email: j.dennis@qmul.ac.uk)

Notes

The authors declare no competing financial interest.

ACKNOWLEDGMENT

X. Zhao, T. Liu, X. Hou and Z. Liu thank the China Scholarship Council for funding.

REFERENCES

(1) Mukherjee, B.; Mukherjee, M.; Choi, Y.; Pyo, S. Control over Multifunctionality in Optoelectronic Device Based on Organic Phototransistor. *ACS Appl. Mater. Interfaces* **2010**, *2* (6), 1614–1620.

(2) Someya, T.; Sekitani, T.; Iba, S.; Kato, Y.; Kawaguchi, H.; Sakurai, T. A Large-Area, Flexible Pressure Sensor Matrix with Organic Field-Effect Transistors for Artificial Skin Applications. *Proc. Natl. Acad. Sci. U. S. A.* **2004**, *101* (27), 9966–9970.

(3) Zhao, X.; Liu, T.; Cui, Y.; Hou, X.; Liu, Z.; Dai, X.; Kong, J.; Shi, W.; Dennis, T. J. S. Antisolvent-Assisted Controllable Growth of Fullerene Single Crystal Microwires for Organic Field Effect Transistors and Photodetectors. *Nanoscale* **2018**, *10* (17), 8170–8179.

(4) Klauk, H.; Zschieschang, U.; Pflaum, J.; Halik, M. Ultralow-Power Organic Complementary Circuits. *Nature* **2007**, *445* (7129), 745–748.

(5) Clark, J.; Lanzani, G. Organic Photonics for Communications. *Nat. Photonics* **2010**, *4* (7), 438–446.

(6) Guo, Y.; Yu, G.; Liu, Y. Functional Organic Field-Effect Transistors. *Adv. Mater.* **2010**, *22* (40), 4427–4447.

(7) Dimitrakopoulos, C. D.; Malenfant, P. R. L. Organic Thin Film Transistors for Large Area Electronics. *Adv. Mater.* **2002**, *14* (2), 99–117.

(8) Baeg, K. J.; Binda, M.; Natali, D.; Caironi, M.; Noh, Y. Y. Organic Light Detectors: Photodiodes and Phototransistors. *Adv. Mater.* **2013**, *25* (31), 4267–4295.

(9) Cicoira, F.; Santato, C. Organic Light Emitting Field Effect Transistors: Advances and Perspectives. *Adv. Funct. Mater.* **2007**, *17* (49), 3421–3434.

(10) Di, C. A.; Zhang, F.; Zhu, D. Multi-Functional Integration of Organic Field-Effect Transistors (OFETs): Advances and Perspectives. *Adv. Mater.* **2013**, *25* (3), 313–330.

(11) Podzorov, V.; Menard, E.; Borissov, A.; Kiryukhin, V.; Rogers, J. A.; Gershenson, M. E. Intrinsic Charge Transport on the Surface of Organic Semiconductors. *Phys. Rev. Lett.* **2004**, *93* (8), 86602.

(12) Zhao, X.; Liu, T.; Zhang, Y.; Wang, S.; Li, X.; Xiao, Y.; Hou, X.; Liu, Z.; Shi, W.; Dennis, T. J. S. Organic Single-Crystalline Donor–Acceptor Heterojunctions with Ambipolar Band-Like Charge Transport for Photovoltaics. *Adv. Mater. Interfaces* **2018**, *5* (14), 1800336.

(13) Zhao, X.; Liu, T.; Shi, W.; Hou, X.; Liu, Z.; Dennis, T. J. S. Understanding Charge Transport in Endohedral Fullerene Single-Crystal Field-Effect Transistors. *J. Phys. Chem. C* **2018**, *122* (16), 8822–8828.

(14) Zhao, X.; Liu, T.; Hou, X.; Liu, Z.; Shi, W.; Dennis, T. J. S. [60]PCBM Single Crystals: Remarkably Enhanced Band-like Charge Transport, Broadband UV-

Visible-NIR Photo-Responsivity and Improved Long-Term Air-Stability. *J. Mater. Chem. C* **2018**, *6* (20), 5489–5496.

(15) Li, H.; Fan, C.; Fu, W.; Xin, H. L.; Chen, H. Solution-Grown Organic Single-Crystalline Donor-Acceptor Heterojunctions for Photovoltaics. *Angew. Chemie - Int. Ed.* **2015**, *54* (3), 956–960.

(16) Bonaccorso, F.; Sun, Z.; Hasan, T.; Ferrari, A. C. Graphene Photonics and Optoelectronics. *Nat. Photonics* **2010**, *4* (9), 611–622.

(17) Wang, Q. H.; Kalantar-Zadeh, K.; Kis, A.; Coleman, J. N.; Strano, M. S. Electronics and Optoelectronics of Two-Dimensional Transition Metal Dichalcogenides. *Nat. Nanotechnol.* **2012**, *7* (11), 699–712.

(18) Yamamura, A.; Watanabe, S.; Uno, M.; Mitani, M.; Mitsui, C.; Tsurumi, J.; Isahaya, N.; Kanaoka, Y.; Okamoto, T.; Takeya, J. Wafer-Scale, Layer-Controlled Organic Single Crystals for High-Speed Circuit Operation. *Sci. Adv.* **2018**, *4* (2), eaao5758.

(19) Zhang, Y.; Dong, H.; Tang, Q.; Ferdous, S.; Liu, F.; Mannsfeld, S. C. B.; Hu, W.; Briseno, A. L. Organic Single-Crystalline P-N Junction Nanoribbons. *J. Am. Chem. Soc.* **2010**, *132* (33), 11580–11584.

(20) Wu, J.; Fan, C.; Xue, G.; Ye, T.; Liu, S.; Lin, R.; Chen, H.; Xin, H. L.; Xiong, R.-G.; Li, H. Interfacing Solution-Grown C60 and (3-Pyrrolinium)(CdCl3) Single Crystals for High-Mobility Transistor-Based Memory Devices. *Adv.*

Mater. **2015**, *27* (30), 4476–4480.

(21) Qin, Y.; Cheng, C.; Geng, H.; Wang, C.; Hu, W.; Xu, W.; Shuai, Z.; Zhu, D. Efficient Ambipolar Transport Properties in Alternate Stacking Donor–acceptor Complexes: From Experiment to Theory. *Phys. Chem. Chem. Phys.* **2016**, *18* (20), 14094–14103.

(22) Zhang, Y.; Dong, H.; Tang, Q.; He, Y.; Hu, W. Mobility Dependence on the Conducting Channel Dimension of Organic Field-Effect Transistors Based on Single-Crystalline Nanoribbons. *J. Mater. Chem.* **2010**, *20* (33), 7029.

(23) Cui, Q. H.; Jiang, L.; Zhang, C.; Zhao, Y. S.; Hu, W.; Yao, J. Coaxial Organic P-N Heterojunction Nanowire Arrays: One-Step Synthesis and Photoelectric Properties. *Adv. Mater.* **2012**, *24* (17), 2332–2336.

(24) Fan, C.; Zoombelt, A. P.; Jiang, H.; Fu, W.; Wu, J.; Yuan, W.; Wang, Y.; Li, H.; Chen, H.; Bao, Z. Solution-Grown Organic Single-Crystalline P-N Junctions with Ambipolar Charge Transport. *Adv. Mater.* **2013**, *25* (40), 5762–5766.

(25) Zhang, J.; Tan, J.; Ma, Z.; Xu, W.; Zhao, G.; Geng, H.; Di, C.; Hu, W.; Shuai, Z.; Singh, K.; et al. Fullerene/Sulfur-Bridged Annulene Cocrystals: Two-Dimensional Segregated Heterojunctions with Ambipolar Transport Properties and Photoresponsivity. *J. Am. Chem. Soc.* **2013**, *135* (2), 558–561.

(26) Zhang, H.; Jiang, L.; Zhen, Y.; Zhang, J.; Han, G.; Zhang, X.; Fu, X.; Yi, Y.; Xu, W.; Dong, H. Organic Cocrystal Photovoltaic Behavior: A Model System to

Study Charge Recombination of C60 and C70 at the Molecular Level. *Adv. Electron. Mater.* **2016**, *2* (6), 1500423.

(27) Xue, G.; Fan, C.; Wu, J.; Liu, S.; Liu, Y.; Chen, H.; Xin, H. L.; Li, H. Ambipolar Charge Transport of TIPS-Pentacene Single-Crystals Grown from Non-Polar Solvents. *Mater. Horiz.* **2015**, *2* (3), 344–349.

(28) Li, H.; Tee, B. C. K.; Cha, J. J.; Cui, Y.; Chung, J. W.; Lee, S. Y.; Bao, Z. High-Mobility Field-Effect Transistors from Large-Area Solution-Grown Aligned C60 Single Crystals. *J. Am. Chem. Soc.* **2012**, *134* (5), 2760–2765.

(29) Zhang, F.; Shi, W.; Luo, J.; Pellet, N.; Yi, C.; Li, X.; Zhao, X.; Dennis, T. J. S.; Li, X.; Wang, S.; et al. Isomer-Pure Bis-PCBM-Assisted Crystal Engineering of Perovskite Solar Cells Showing Excellent Efficiency and Stability. *Adv. Mater.* **2017**, *29* (17), 1606806.

(30) Lloyd, M. T.; Mayer, A. C.; Tayi, A. S.; Bowen, A. M.; Kasen, T. G.; Herman, D. J.; Mourey, D. A.; Anthony, J. E.; Malliaras, G. G. Photovoltaic Cells from a Soluble Pentacene Derivative. *Org. Electron.* **2006**, *7* (5), 243–248.

(31) Shi, W.; Hou, X.; Liu, T.; Zhao, X.; Sieval, A. B.; Hummelen, J. C.; Dennis, T. J. S. Purification and Electronic Characterisation of 18 Isomers of the OPV Acceptor Material Bis-[60] PCBM. *Chem. Commun.* **2017**, *53* (5), 975–978.

(32) Schulze, K.; Uhrich, C.; Schüppel, R.; Leo, K.; Pfeiffer, M.; Brier, E.; Reinold, E.; Bäuerle, P. Efficient Vacuum-Deposited Organic Solar Cells Based on a New

Low-Bandgap Oligothiophene and Fullerene C60. *Adv. Mater.* **2006**, *18* (21), 2872–2875.

(33) Di, D.; Yang, L.; Richter, J. M.; Meraldi, L.; Altamimi, R. M.; Alyamani, A. Y.; Credgington, D.; Musselman, K. P.; MacManus-Driscoll, J. L.; Friend, R. H. Efficient Triplet Exciton Fusion in Molecularly Doped Polymer Light-Emitting Diodes. *Adv. Mater.* **2017**, *29* (13), 1605987.

(34) Deng, W.; Jie, J.; Shang, Q.; Wang, J.; Zhang, X.; Yao, S.; Zhang, Q.; Zhang, X. Organic Nanowire/crystalline Silicon P - N Heterojunctions for High-Sensitivity, Broadband Photodetectors. *ACS Appl. Mater. Interfaces* **2015**, *7* (3), 2039–2045.

(35) Wu, J.; Li, Q.; Xue, G.; Chen, H.; Li, H. Preparation of Single-Crystalline Heterojunctions for Organic Electronics. *Adv. Mater.* **2017**, *29* (14), 1606101.

(36) Anthony, J. E.; Brooks, J. S.; Eaton, D. L.; Parkin, S. R. Functionalized Pentacene: Improved Electronic Properties from Control of Solid-State Order. *J. Am. Chem. Soc.* **2001**, *123* (38), 9482–9483.

(37) David, W. I. F.; Ibberson, R. M.; Matthewman, J. C.; Prassides, K.; Dennis, T. J. S.; Hare, J. P.; Kroto, H. W.; Taylor, R.; Walton, D. R. M. Crystal Structure and Bonding of Ordered C60. *Nature* **1991**, *353* (6340), 147–149.

(38) Baeg, K. J.; Kim, J.; Khim, D.; Caironi, M.; Kim, D. Y.; You, I. K.; Quinn, J. R.; Facchetti, A.; Noh, Y. Y. Charge Injection Engineering of Ambipolar Field-

Effect Transistors for High-Performance Organic Complementary Circuits. *ACS Appl. Mater. Interfaces* **2011**, *3* (8), 3205–3214.

(39) Tang, Q.; Li, H.; Liu, Y.; Hu, W. High-Performance Air-Stable N-Type Transistors with an Asymmetrical Device Configuration Based on Organic Single-Crystalline Submicrometer/nanometer Ribbons. *J. Am. Chem. Soc.* **2006**, *128* (45), 14634–14639.

(40) Park, K. S.; Lee, K. S.; Kang, C. M.; Baek, J.; Han, K. S.; Lee, C.; Koo Lee, Y. E.; Kang, Y.; Sung, M. M. Cross-Stacked Single-Crystal Organic Nanowire P-N Nanojunction Arrays by Nanotransfer Printing. *Nano Lett.* **2015**, *15* (1), 289–293.

(41) Chen, S.; Teng, C.; Zhang, M.; Li, Y.; Xie, D.; Shi, G. A Flexible UV–Vis–NIR Photodetector Based on a Perovskite/Conjugated-Polymer Composite. *Adv. Mater.* **2016**, 5969–5974.

(42) Chen, G.; Liang, B.; Liu, X.; Liu, Z.; Yu, G.; Xie, X.; Luo, T.; Chen, D.; Zhu, M.; Shen, G.; et al. High-Performance Hybrid Phenyl-C61-Butyric Acid Methyl Ester/Cd3P2nanowire Ultraviolet-Visible-near Infrared Photodetectors. *ACS Nano* **2014**, *8* (1), 787–796.

(43) Park, S.; Kim, S. J.; Nam, J. H.; Pitner, G.; Lee, T. H.; Ayzner, A. L.; Wang, H.; Fong, S. W.; Vosgueritchian, M.; Park, Y. J.; et al. Significant Enhancement of Infrared Photodetector Sensitivity Using a Semiconducting Single-Walled Carbon nanotube/C60 Phototransistor. *Adv. Mater.* **2015**, *27* (4), 759–765.

(44) Wei, L.; Yao, J.; Fu, H. Solvent-Assisted Self-Assembly of Fullerene into Single-Crystal Ultrathin Microribbons as Highly Sensitive UV–visible Photodetectors. *ACS Nano* **2013**, *7* (9), 7573–7582.

(45) Wu, G.; Chen, C.; Liu, S.; Fan, C.; Li, H.; Chen, H. Solution-Grown Organic Single-Crystal Field-Effect Transistors with Ultrahigh Response to Visible-Blind and Deep UV Signals. *Adv. Electron. Mater.* **2015**, *1* (8), 1500136.

(46) Noh, Y.-Y.; Kim, D.-Y.; Yase, K. Highly Sensitive Thin-Film Organic Phototransistors: Effect of Wavelength of Light Source on Device Performance. *J. Appl. Phys.* **2005**, *98* (7), 74505.

(47) Saragi, T. P. I.; Londenberg, J.; Salbeck, J. Photovoltaic and Photoconductivity Effect in Thin-Film Phototransistors Based on a Heterocyclic Spiro-Type Molecule. *J. Appl. Phys.* **2007**, *102* (4), 46104.

(48) Saragi, T. P. I.; Pudzich, R.; Fuhrmann, T.; Salbeck, J. Organic Phototransistor Based on Intramolecular Charge Transfer in a Bifunctional Spiro Compound. *Appl. Phys. Lett.* **2004**, *84* (13), 2334–2336.

(49) Noh, Y.-Y.; Ghim, J.; Kang, S.-J.; Baeg, K.-J.; Kim, D.-Y.; Yase, K. Effect of Light Irradiation on the Characteristics of Organic Field-Effect Transistors. *J. Appl. Phys.* **2006**, *100* (9), 94501.

(50) Noh, Y.-Y.; Kim, D.-Y.; Yoshida, Y.; Yase, K.; Jung, B.-J.; Lim, E.; Shim, H.-K. High-Photosensitivity P-Channel Organic Phototransistors Based on a

Biphenyl End-Capped Fused Bithiophene Oligomer. *Appl. Phys. Lett.* **2005**, *86* (4), 43501.

(51) O'Brien, G. A.; Quinn, A. J.; Tanner, D. A.; Redmond, G. A Single Polymer Nanowire Photodetector. *Adv. Mater.* **2006**, *18* (18), 2379–2383.

(52) Zhang, B. Y.; Liu, T.; Meng, B.; Li, X.; Liang, G.; Hu, X.; Wang, Q. J. Broadband High Photoresponse from Pure Monolayer Graphene Photodetector. *Nat. Commun.* **2013**, *4*, 1811.

(53) Tsai, W. W.; Chao, Y. C.; Chen, E. C.; Zan, H. W.; Meng, H. F.; Hsu, C. S. Increasing Organic Vertical Carrier Mobility for the Application of High Speed Bilayered Organic Photodetector. *Appl. Phys. Lett.* **2009**, *95* (21), 306.

(54) Ramuz, M.; Bürgi, L.; Winnewisser, C.; Seitz, P. High Sensitivity Organic Photodiodes with Low Dark Currents and Increased Lifetimes. *Org. Electron. physics, Mater. Appl.* **2008**, *9* (3), 369–376.

(55) Ng, T. N.; Wong, W. S.; Chabinyc, M. L.; Sambandan, S.; Street, R. A. Flexible Image Sensor Array with Bulk Heterojunction Organic Photodiode. *Cit. Appl. Phys. Lett. Rev. Sci. Instrum. Appl. Phys. Lett* **2008**, *92* (91), 213303–213311.

(56) Hamasaki, T.; Morimune, T.; Kajii, H.; Minakata, S.; Tsuruoka, R.; Nagamachi, T.; Ohmori, Y. Fabrication and Characteristics of Polyfluorene Based Organic Photodetectors Using Fullerene Derivatives. *Thin Solid Films* **2009**, *518* (2), 548–550.

(57) Gong, X.; Tong, M.; Xia, Y.; Cai, W.; Moon, J. S.; Cao, Y.; Yu, G.; Shieh, C. L.; Nilsson, B.; Heeger, A. J. High-Detectivity Polymer Photodetectors with Spectral Response from 300 Nm to 1450 Nm. *Science.* **2009**, *325* (5948), 1665–1667.

(58) Yao, Y.; Liang, Y.; Shrotriya, V.; Xiao, S.; Yu, L.; Yang, Y. Plastic near-Infrared Photodetectors Utilizing Low Band Gap Polymer. *Adv. Mater.* **2007**, *19* (22), 3979–3983.

(59) Zhang, J.; Geng, H.; Virk, T. S.; Zhao, Y.; Tan, J.; Di, C. A.; Xu, W.; Singh, K.; Hu, W.; Shuai, Z.; et al. Sulfur-Bridged Annulene-TCNQ Co-Crystal: A Self-Assembled molecular Level Heterojunction'' with Air Stable Ambipolar Charge Transport Behavior. *Adv. Mater.* **2012**, *24* (19), 2603–2607.

(60) Qin, Y.; Zhang, J.; Zheng, X.; Geng, H.; Zhao, G.; Xu, W.; Hu, W.; Shuai, Z.; Zhu, D. Charge-Transfer Complex Crystal Based on Extended-π-Conjugated Acceptor and Sulfur-Bridged Annulene: Charge-Transfer Interaction and Remarkable High Ambipolar Transport Characteristics. *Adv. Mater.* **2014**, *26* (24), 4093–4099.